Macromolecular Research, Vol. 23, No. 2, pp 214-222 (2015)
DOI 10.1007/s13233-015-3035-z

www.springer.com/13233
pISSN 1598-5032 eISSN 2092-7673

2,2-Dimethyl-2*H*-Benzimidazole Based Small Molecules for Organic Solar Cells

Juae Kim[1], Joo Young Shim[1], Seyeong Song[2], Jinwoo Kim[1], Il Kim[3], Jin Young Kim[2], and Hongsuk Suh*[,1]

[1]*Department of Chemistry and Chemistry Institute for Functional Materials, Pusan National University, Busan 609-735, Korea*
[2]*Interdisciplinary School of Green Energy, Ulsan National Institute of Science and Technology, Ulsan 689-798, Korea*
[3]*The WCU Center for Synthetic Polymer Bioconjugate Hybrid Materials, Department of Polymer Science and Engineering, Pusan National University, Busan 609-735, Korea*

Received October 19, 2014; Revised December 12, 2014; Accepted December 13, 2014

Abstract: We report the small molecules utilizing new electron-deficient unit, 2,2-dimethyl-2*H*-benzimidazole (MBI) and phenanthro[9,10-*c*][1,2,5]thiadiazole (PT), for the photovoltaic application. Donor-acceptor-donor (D-A-D) types of conjugated small molecules containing benzo[1,2-*b*;3,4-*b*′]dithiophene (BDT) as electron rich unit and MBI and PT as electron deficient units (**SM1** and **SM2**) were synthesized. D-A-D type of small molecules has the abilities of increasing intramolecular charge transfer (ICT) inducing long wavelength absorption and lowering the HOMO level for the improvement of open-circuit voltage (V_{OC}). **SM1** was synthesized by coupling BDT and PT units by Stille coupling reaction with Pd(0)-catalyst. By using same type of Pd(0)-catalized reaction, BDT unit and MBI unit linked with two thiophenes were coupled to provide **SM2**. The spectrum of **SM2** in the solid thin film shows absorption band with maximum peak at 601 nm and the absorption onset at 756 nm, corresponding to band gap of 1.64 eV. The device comprising **SM2** with PCBM (3:7) showed a V_{OC} of 0.62 V, a J_{SC} of 1.69 mA/cm^2, and a fill factor (FF) of 0.27, giving a power conversion efficiency of 0.28%.

Keywords: small molecule, photovoltaic cells, benzodithiophene, 2,2-dimethyl-2*H*-benzimidazole.

Introduction

For the realization of the organic solar cells, the bulk heterojunction structure have been investigated intensively over recent several years especially caused by their advantages such as flexibility, large area fabrication, low cost, light weight, and loll-to loll processibility.[1-4]

Even though, researches of organic solar cells (OSCs) based on conjugated polymers have brought improved PCE up to 7-10%, small molecules have been investigated extensively caused by the advantages of well defined molecular structure, definite molecular weight and high purity of the material for the credible reproducibility of the device performance.[5]

In the desperate endeavor to highlight the bright points of the small molecules, various kinds of combination of the electron rich/deficient units, triphenylamine,[6] oligothiophene,[7] diketopyrrolopyrrole,[8,9] 2,1,3-benzothiadiazole,[10,11] 1,2,5-thiadiazolo[3,4-*c*]pyridine[12] and dithienosilole[13] have been reported.[3]

To improve the low solubility of the well established 2,1,3-benzothiadiazole (BT) unit, 2,2-dimethyl-2*H*-benzimidazole (MBI), electron deficient units, has been designed and utilized for the intramolecular charge transfer (ICT) in our previous study (Figure 1). MBI replaced the sulfur at 2-position of BT unit with dialkyl substituted carbon to maintain the 1,2-quinoid form and provide a high solubility.[14,15] With PT unit, it was intended to expend the planarity for the enhancement of π-stacking with a penetrating fullerene network in the blended system[16,17] for the generation of higher charge carrier mobility to improve the short circuit current (J_{SC}).[18]

Benzo[1,2-*b*;3,4-*b*′]dithiophene (BDT) including a rigid and coplanar fused ring system has highly extended conjugated system for the improvement of π-stacking. Even though it has been shown that conjugated polymers and small molecules containing BDT unit provide high charge carrier mobilities, there has been not many reports on small molecules with BDT for OSCs.

In this paper, we report conjugated oligomers, **SM1** and **SM2**, containing D-A-D types of organic small molecules with BDT as donor (D) unit and MBI and PT (phenanthro[9,10-*c*][1,2,5]thiadiazole) as acceptor (A) units (Scheme I).[3]

D-A type small molecules have the abilities of increasing the effect of ICT causing long wavelength absorbance and

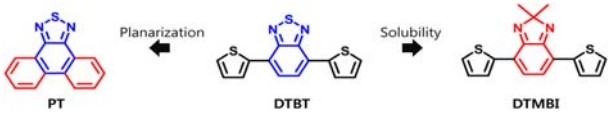

Figure 1. Approach towards acceptor monomer.

*Corresponding Author. E-mail: hssuh@pusan.ac.kr

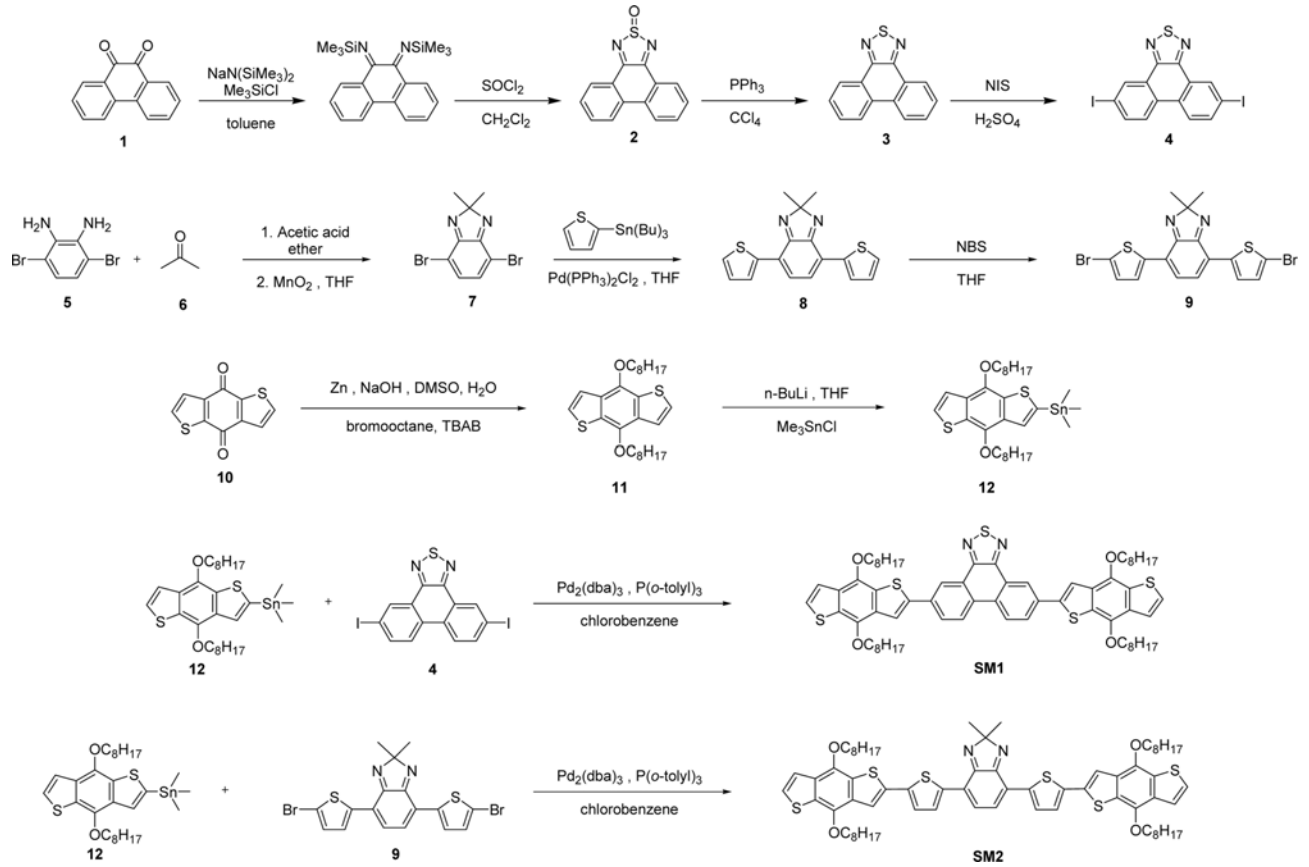

Scheme I. Synthetic route for the synthesis of the monomers and small molecules.

also lowering the highest occupied molecular orbital (HOMO) level for the enhanced open-circuit voltage (V_{OC}). By using the Stille coupling condition, BDT and MBI/PT fragments were incorporated to synthesize 1,1-bis(4,8-dioctylbenzo[1,2-*b*:4,5-*b*′]dithiophene)-4′,7′-di-2-thienyl-2,2-dimethyl-2*H*-benzimidazole (**SM1**) and 1,1-bis(4,8-dioctylbenzo[1,2-*b*:4,5-*b*′]dithiophene)-5′,10′-phenanthro[9,10-*c*] [1,2,5] thiadiazole (**SM2**), respectively. Novel conjugated small molecules, **SM1** and **SM2**, showed good solubility at room temperature in various organic solvents. The photovoltaic properties of the small molecules were investigated by fabrication of the polymer solar cells with the configuration of ITO (indium tin oxide)/PEDOT:PSS (poly(3,4-ethylenedioxythiophene):poly(styrene sulfonate))/small molecule: PCBM ([6,6]-phenyl C60 butyric acid methyl ester)/Al.

Experimental

Instrumental Characterization. All reagents were purchased from Aldrich or TCI, and used without further purification. Solvents were purified by normal procedure and handled under moisture-free atmosphere. ^{1}H and ^{13}C nuclear magnetic resonance (NMR) spectra were recorded with a Varian Gemini-300 (300 MHz) spectrometer and chemical shifts were recorded in ppm units with TMS as the internal standard. Flash column chromatography was performed with Merck silica gel 60 (particle size 230-400 mesh ASTM) with ethyl acetate/hexane or methanol/methylene chloride gradients unless otherwise indicated. Analytical thin layer chromatography (TLC) was conducted using Merck 0.25 mm silica gel 60F pre-coated aluminum plates with fluorescent indicator UV254. High-resolution mass spectra (HRMS) were recorded on a JEOL JMS-700 mass spectrometer under electron impact (EI) conditions in the Korea Basic Science Institute (Daegu). The ultraviolet-visible (UV-vis) absorption spectra were recorded by a Varian 5E UV/VIS/NIR spectrophotometer. The atomic force microscope (AFM) instrumentation consisted of a Veeco NanoScope AFM and standard silicon cantilever (Veeco; tip radius, 8 nm; normal spring constant, 21-78 N/m; scan rate, 2.0 Hz) at ambient conditions (in air, 20 ºC).

Device Fabrication and Measurements. Solar cells were fabricated on an indium tin oxide (ITO)-coated glass substrate with the following structure; ITO-coated glass substrate/poly (3,4-ethylenedioxythiophene) (PEDOT:PSS)/small molecule: PCBM/Al. The ITO-coated glass substrate was first cleaned with detergent, ultrasonicated in acetone and isopropyl alcohol, and subsequently dried overnight in an oven. PEDOT:PSS (Baytron PH) was spin-cast from aqueous solution to form a

film of 40 nm thickness. The substrate was dried for 10 min at 140 ºC in air and then transferred into a glove box to spin-cast the active layer. A solution containing a mixture of small molecule:PCBM in dichlorobenzene solvent with concentration of 33 mg/mL was then spin-cast on top of the PEDOT/PSS layer. The sample was heated at 80 ºC for 10 min in air. Then, an aluminum (Al, 100 nm) electrode was deposited by thermal evaporation in a vacuum of about 5×10^{-7} Torr. Current density-voltage (*J-V*) characteristics of the devices were measured using a Keithley 236 Source Measure Unit. Solar cell performance utilized an Air Mass 1.5 Global (AM 1.5 G) solar simulator with an irradiation intensity of 1000 W m^{-2}. An aperture (12.7 mm^2) was used on top of the cell to eliminate extrinsic effects such as cross-talk, waveguiding, shadow effects, *etc*. The spectral mismatch factor was calculated by comparison of solar simulator spectrum with AM 1.5 spectrum at room temperature. In order to check the photocurrent of devices, incident photon-to-current collection efficiency (IPCE) was measured by using a solar cell spectral response measurement system (PV Measurement Inc.). The silicon calibration photo-diode I772 was used for spectral calibration before measuring IPCE of devices. The IPCE is a measure of the photon to electron conversion efficiency at a particular irradiation wavelength (eq. (1)).

$$\text{IPCE} = (1240\times J_{SC}) / (\lambda_i \times P_{in}) \quad (1)$$

Synthesis of Monomers and Small Molecules.

Synthesis of Phenanthro[9,10-c][1,2,5]thiadiazole 2-oxide (2): To a stirred solution of 9,10-phenanthrenequinone (**1**) (6 g, 28.8 mmol) in 200 mL of toluene at 50 ºC under argon was added dropwise of 1 M $NaN(Me_3Si)_2$ (86.4 mL, 86.4 mmol) solution in CH_2Cl_2. After 30 min, Me_3SiCl (10.9 mL, 86.4 mmol) was added. The reaction mixture was refluxed for 10 h. Then, the reaction mixture was cooled to room temperature. After removing the solvent under reduced pressure, the residue was redissolved in CH_2Cl_2 at room temperature. After adding 5 mL of $SOCl_2$, slowly, the reaction mixture was refluxed. After cooling the reaction mixture, the reaction mixture was treated with 200 mL of water. The aqueous phase was extracted with CH_2Cl_2 and combined organic layer was dried over $MgSO_4$. After removing the solvent under reduced pressure, the residue was purified by flash to give 3 g (33%) of compound **2** as a yellow solid; mp 165.2 ºC; ^{1}H NMR (300 MHz, $CDCl_3$) δ (ppm) 7.57 (t, 2H, *J*=8.0), 7.81 (t, 2H, *J*=7.4 Hz), 8.22 (d, 2H, *J*=8.2 Hz), 8.52 (d, 2H, *J*=7.9 Hz); ^{13}C NMR (75 MHz, $CDCl_3$) δ (ppm) 111.2, 115.9, 124.6, 125.1, 129.8, 130.5, 135.6; HRMS (EI^+, m/z) calcd for $C_{14}H_8N_2OS$ 252.0357, found 252.0360.

Synthesis of Phenanthro[9,10-c][1,2,5]thiadiazole (3): To the solution of phenanthro[9,10-*c*][1,2,5]thiadiazole 2-oxide (**2**) (3.5 g, 13.9 mmol) in CH_2Cl_2 at 0 ºC, was added PPh_3 (10.9 g, 41.6 mmol). After refluxing for overnight, the reaction mixture was cooled and treated with 200 mL of water. The aqueous phase was separated and extracted with CH_2Cl_2. After drying the combined organic layer over $MgSO_4$, the solvent was removed under reduced pressure. The residue was purified by flash chromatography to give 2.23 g (33%) of compound **3** as a white solid; mp 165.2 ºC; ^{1}H NMR (300 MHz, $CDCl_3$) δ (ppm) 7.70 (t, 2H, *J*=7.5 Hz), 7.73 (t, 2H, *J*=7.5 Hz), 8.50 (d, 2H, *J*=7.4 Hz), 8.72 (d, 2H, *J*=7.4 Hz); ^{13}C NMR (75 MHz, $CDCl_3$) δ (ppm) 123.4, 126.0, 126.2, 128.1, 129.6, 131.5, 153.3; HRMS (EI^+, m/z) calcd for $C_{14}H_8N_2S$ 237.0486, found 237.0487.

Synthesis of 5,10-Diiodophenanthro[9,10-c][1,2,5]thiadiazole (4): To a stirred solution of phenanthro[9,10-*c*][1,2,5]thiadiazole (**3**) (3 g, 12.7 mmol) in 80 mL of H_2SO_4 at room temperature under argon was added *N*-iodosuccinimide (NIS) (5.99 g, 26.6 mmol). After stirring for 1 h at room temperature, the reaction mixture was quenched with 200 mL of water. The reaction mixture was cooled down and resulting yellow solid was collected by filtration. Recrystallization from THF afforded to 5.95 g (96%) of compound **4** as a yellow solid; mp 227.7 ºC; ^{1}H NMR (300 MHz, $CDCl_3$) δ (ppm) 8.04 (d, 2H, *J*=6.9 Hz), 8.20 (d, 2H, *J*=8.5 Hz), 9.08 (s, 2H); ^{13}C NMR was not measured due to very low solubility; HRMS (EI^+, m/z) calcd for $C_{14}H_6I_2N_2S$ 487.8341, found 487.8343.

Synthesis of 4,7-Dibromo-2,2-dimethyl-2*H*-benzimidazole (7): A solution of 3,6-dibromobenzene-1,2-diamine (**5**) (10 g, 37.65 mmol), acetone (**6**) (10 mL), acetic acid (10 mL), and diethyl ether (200 mL) was heated at 50 ºC overnight. After cooling to room temperature, the reaction mixture was treated with water and ethyl acetate. The aqueous phase was extracted with ethyl acetate and combined organic layer was dried with $MgSO_4$. After concentration of the organic phase under reduced pressure, the residue was purified by column chromatography to give 4,7-dibromo-2,2-dimethyl-2,3-dihydro-1*H*-benzimidazole. To a stirred solution of 4,7-dibromo-2,2-dimethyl-2,3-dihydro-1*H*-benzimidazole in 50 mL of tetrahydrofuran (THF) at room temperature was added MnO_2 (7.4 g, 85 mmol). After 3 h at room temperature, the solid was filtered and washed with several batches of THF. The combined organic phase was concentrated under reduced pressure and purified by flash column chromatography to give 3.2 g (28%) of 4,7-dibromo-2,2-dimethyl-2*H*-benzimidazole (**7**) as yellow powder. mp 132 ºC; ^{1}H NMR (300 MHz, Acetone-d_6) δ (ppm) 1.52 (s, 6H), 6.49 (s, 2H); ^{13}C NMR (75 MHz, Acetone-d_6) δ (ppm) 79.6, 98.3, 121.7, 121.8, 139.6; HRMS (EI^+, *m/z*) calcd for $C_9H_8N_2Br_2$ 301.9054, found 301.9056.

Synthesis of 2,2-Dimethyl-4,7-di(2-thienyl)-2*H*-benzimidazole (8): To a stirred solution of 4,7-dibromo-2,2-dimethyl-2*H*-benzimidazole (**7**) (2.7 g, 8.9 mmol) and tributyl(2-thienyl)stannane (16.6 g, 44.4 mmol) in 40 mL of THF at room temperature was added dichlorobis(triphenylphosphine)palladium(II) (2 mol%). The reaction mixture was stirred for 12 h at 80 ºC, concentrated under reduced pressure, and purified by flash column chromatography to give 1.4 g (51%) of 2,2-dimethyl-4,7-di(2-thienyl)-2*H*-benzimidazole (**8**) as red solid. mp 172 ºC; ^{1}H NMR (300 MHz, $CDCl_3$) δ (ppm) 1.67 (s, 6H), 7.13 (t, 2H, *J*=3.8 Hz), 7.30 (s, 2H), 7.38 (d, 2H. *J*=4.9 Hz), 8.03 (d, 2H, *J*=3.5 Hz); ^{13}C NMR (75 MHz, $CDCl_3$) δ (ppm) 22.3

105.4, 126.8, 128.2, 128.2, 128.8, 128.9, 138.9, 157.9. HRMS (EI^+, *m/z*) calcd for $C_{17}H_{14}N_2S_2$ 310.0598, found 310.0600.

Synthesis of 4,7-Bis(5-bromo-2-thienyl)-2,2-dimethyl-2*H*-benzimidazole (9): To a stirred solution of 2,2-dimethyl-4,7-di(2-thienyl)-2*H*-benzimidazole (**8**) (1.3 g, 4.19 mmol) in THF at room temperature was added *N*-bromosuccinimide (NBS) (1.52 g, 8.6 mmol). After 3 h at room temperature, water and ethyl acetate was added. The organic phase was washed with 3×100 mL of water. The organic phase was concentrated under reduced pressure and purified by flash column chromatography to give 1.25 g (64%) of compound **5** as red solid. mp 207 °C; ^{1}H NMR (300 MHz, $CDCl_3$): δ (ppm) 1.58 (s, 6H), 7.08 (d, 2H, *J*=3.9 Hz), 7.21 (s, 2H), 7.69 (d, 2H, *J*=3.9 Hz); ^{13}C NMR (75 MHz, $CDCl_3$): δ (ppm) 22.0, 105.5, 115.1, 127.5, 127.9, 128.0, 130.7, 139.8, 157.4; HRMS (EI^+, *m/z*) calcd for $C_{17}H_{12}Br_2N_2S_2$ 465.8809, found 465.8810.

Synthesis of 4,8-Dioctyloxybenzo[1,2-b;3,4-b]dithiophene (11): Compound **10** (4.4 g, 20 mmol), zinc powder (2.86 g, 44 mmol), 40 mL of water, and 40 mL of DMSO (dimethyl sulfoxide) were put into a 250 mL flask; then 12 g of NaOH was added into the mixture. The mixture was well stirred and heated to reflux for 1 h. Then, 1-bromooctane (15 g, 60 mmol) and a catalytic amount of tetrabutylammonium bromide were added into the flask. After being refluxed for 2 h, the color of the reaction mixture was red to deep red and additional amount of zinc powder (1.3 g, 20 mmol) was added to the reaction mixture. After reflux for additional 6 h, the reaction mixture, with yellow to orange color, was cooled and poured into cold water and extracted with 2×200 mL of diethyl ether. The combined ether layer was dried over anhydrous $MgSO_4$. After concentration, the residue was purified by recrystallization from ethyl alcohol two times. Recrystallization afforded to 9.26 g (83%) of compound **11** as colorless crystal. mp 47.5 °C; ^{1}H NMR (300 MHz, $CDCl_3$): δ (ppm) 0.90 (t, 6H, *J*=6.6 Hz), 1.36 (m, 24H), 4.28 (t, 4H, *J*=6.6 Hz), 7.37 (d, 2H, *J*=5.5 Hz), 7.48 (d, 2H, *J*=5.5Hz); ^{13}C NMR (75 MHz, $CDCl_3$): δ (ppm) 14.3, 22.9, 26.3, 29.5, 30.0, 32.0, 71.2, 74.2, 120.5, 126.2, 130.4, 131.8, 144.7; HRMS (FAB^+, *m/z*) calcd for $C_{26}H_{38}O_2S_2$ 446.2313, found 446.2315.

Synthesis of 1-Trimethyltin-4,8-dioctylbenzo[1,2-b:4,5-b′] dithiophene (12): Compound **11** (0.62 g, 1.4 mmol) was dissolved in anhydrous THF (20 mL) and cooled to -78 °C using acetone/dry ice bath under argon. To the stirred reaction mixture, butyllithium solution (2.5 M in hexanes, 1.4 mL, 3.5 mmol) was added dropwise. After the addition, the reaction mixture was stirred at -78 °C for 30 min and RT for 30 min. After cooling to -78 °C again, the reaction mixture was treated with trimethyltin chloride solution (1 M in hexanes, 4.2 mL, 4.2 mmol) and stirred at RT for overnight. The reaction mixture was quenched with 50 mL water and extracted with several batches of diethyl ether. The combined organic phase was dried with anhydrous sodium sulfate and concentrated in vacuo. Recrystallization of the residue from isopropanol yielded the compound **12** as colorless needles 0.70 g (65%). mp 67.2 °C; ^{1}H NMR (300 MHz, $CDCl_3$): δ (ppm) 0.46 (s, 9H), 0.90 (t, 6H, *J*=6.9 Hz), 1.3-1.9 (m, 24H), 4.29 (t, 4H, *J*=6.6 Hz), 7.34 (d, 1H, *J*=5.5 Hz), 7.46 (d, 1H, *J*=5.5Hz), 7.53 (s, 1H); HRMS (FAB^+, *m/z*) calcd for $C_{29}H_{46}O_2S_2Sn$ 610.1964, found 610.1964.

Synthesis of 1,1-Bis(4,8-dioctylbenzo[1,2-b:4,5-b']dithiophene)-4',7'-di-2-thienyl-2,2-dimethyl-2H-benzimidazole (SM1): Compound **4** (1 g, 2.05 mmol), compound **12** (3.75 g, 6.15 mmol) and $Pd_2(dba)_3$(3 mol%) were dissolved in toluene. The reaction mixture was stirred for 2 days at 120 °C, concentrated under reduced pressure, and purified by flash column chromatography to give 400 mg of **SM1** as yellow solid; mp 154 °C; ^{1}H NMR (300 MHz, $CDCl_3$): δ (ppm) 0.91 (t, 12H, *J*=6.9 Hz), 1.2-1.6 (m, 40H), 1.94 (q, 8H, *J*=7.4 Hz), 4.1-4.2 (m, 8H), 7.27 (d, 2H, *J*=7.1 Hz), 7.39 (d, 2H, *J*=8.5 Hz), 7.77 (s, 2H), 7.94 (d, 2H, *J*=7.1 Hz), 8.31 (d, 2H, *J*=8.5 Hz), 8.83 (s, 2H); ^{13}C NMR (75 MHz, $CDCl_3$): δ (ppm) 14.4, 23.1, 26.4, 26.4, 29.6, 29.6, 29.8, 29.9, 30.8, 32.2, 73.8, 74.8, 116.4, 120.4, 120.6, 122.7, 123.6, 123.6, 126.1, 126.9, 129.0, 130.3, 132.0, 132.0, 133.5, 142.0, 144.6, 153.2; HRMS (FAB^+, *m/z*) calcd for $C_{66}H_{81}O_4N_2S_5$ 1125.4800, found 1125.4803.

Synthesis of 1,1-Bis(4,8-dioctylbenzo[1,2-b:4,5-b']dithiophene)-5',10'-phenanthro[9,10-c][1,2,5]thiadiazole (SM2): Compound **9** (1 g, 2.14 mmol), compound **12** (3.9 g, 6.41 mmol) and $Pd_2(dba)_3$ (3 mol%) were dissolved in toluene. The reaction mixture was stirred for 2 days at 120 °C, concentrated under reduced pressure, and purified by flash column chromatography to give 400 mg of **SM2** as dark navy solid; mp 124 °C; ^{1}H NMR (300 MHz, $CDCl_3$): δ (ppm) 0.92 (t, 12H, *J*=6.0 Hz), 1.3-1.7 (m, 40H), 1.73 (s, 6H), 1.92 (q, 8H, *J*=6.9 Hz), 4.30 (q, 8H, *J*=6.6 Hz), 7.22 (s, 2H), 7.29 (d, 2H, *J*=3.9 Hz), 7.36 (d, 2H, *J*=5.5 Hz), 7.45 (d, 2H, *J*=5.5 Hz), 7.58 (s, 2H), 7.97 (d, 2H, *J*=3.6 Hz); ^{13}C NMR (75 MHz, $CDCl_3$): δ (ppm) 14.3, 22.4, 22.9, 26.3, 29.5, 29.7, 30.8, 32.1, 74.1, 105.6, 116.8, 120.6, 126.5, 126.3, 128.3, 128.5, 129.2, 129.3, 130,8, 132.3, 132.3, 136.5, 138.9, 139.0, 144.3, 144.7, 157.9; HRMS (FAB^+, *m/z*) calcd for $C_{69}H_{87}O_4N_2S_6$ 1199.4990, found 1199.4994.

Results and Discussion

Synthesis and Characterization. The general synthetic routes toward the intermediate and small molecules are outlined in Scheme I. 1-Trimethyltin-4,8-dioctylbenzo[1,2-*b*:4,5-*b*′]dithiophene (**12**), which was prepared from benzo[1,2-*b*:4,5-*b*'] dithiophene-4,8-dione (**10**) over two steps, and 5,10-diiodophenanthro[9,10-*c*][1,2,5]thiadiazole (**4**),[19] which was prepared from phenanthroquinone (**1**) over four steps, were coupled to provide **SM1** through Stille reaction with Pd(0)-catalyst. By using the same polymerization condition, compound **12** and 4,7-bis(5-bromo-2-thienyl)-2,2-dimethyl-2*H*-benzimidazole (**9**),[14,15] which was synthesized from 3,6-dibromo-1,2-phenylenediamine (**5**) over three steps, provided **SM2**. The structures and purities of all the compounds were confirmed by ^{1}H NMR, ^{13}C NMR, and HRMS.

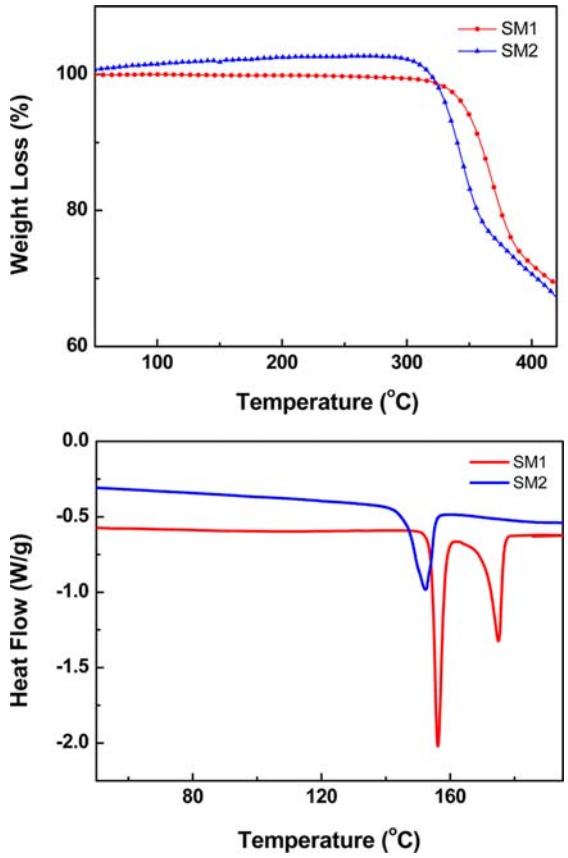

Figure 2. Thermo gravimetric analysis of the small molecules under N_2. Inner: Differential scanning calorimetry of the small molecules under N_2.

Table I. Thermal Properties and Optical Properties of SM1 and SM2

Donor	T_d (°C)	λ_{max} (nm)	
		in Solution	in Thin Film
SM1	346	362	367
SM2	333	368, 581	381, 601

The thermal properties of the small molecules were characterized by both differential scanning calorimetry (DSC) and thermal gravimetric analysis (TGA) as shown in Figure 2 and summarized in Table I. The differential scanning calorimetry analysis was performed on a DSC 822 at heating rates of 10 °C/min. Thermal gravimetric analysis was performed with a Dupont 951 TGA instrument in a nitrogen atmosphere at a heating rate of 10 °C/min to 800 °C. The small molecules showed good thermal stability with onset decomposition temperatures (T_d, 5% weight loss) of 346 and 333 °C, respectively. Both **SM1** and **SM2** did not show discernible glass transition temperature (T_g). **SM1** with PT unit showed higher thermal stability than the case of **SM2**, which is attributed to the PT fragment with the more planar structure. The high thermal stability of the resulting small molecules prevents the deformation of the morphology and is important for OPV (organic photovoltaic) device applications.

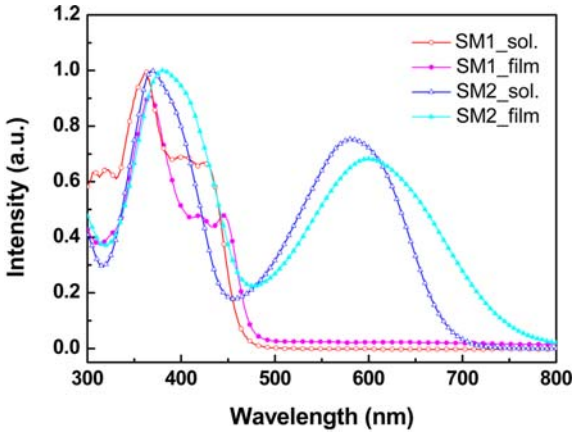

Figure 3. UV-visible absorption spectra of small molecules in chloroform solution and the solid state.

Optical Properties of the Small Molecules. The optical properties of solutions and films of **SM1** and **SM2** were investigated by UV-vis absorption spectroscopy. Uniform film was prepared on quartz plates by spin-casting from their chloroform solution at room temperature. The UV-vis absorption spectra of the small molecules in solution and thin films are shown in Figure 3 and summarized in Table I. The solution and the solid thin film of **SM1** present absorption bands with maximum peaks at 362 and 367 nm, respectively. As compared to this, the solution and the solid thin film of **SM2** provided absorption bands with maximum peaks at 368, 581 and 381, 601 nm, respectively. The short-wavelength absorption peaks, at around 370-380 nm, have been ascribed to a delocalized excitonic π-π* transition in the conjugated chains and the long-wavelength absorption peaks of **SM2**, at around 581 and 601 nm, have been attributed to the intramolecular charge transfer (ICT) between the BDT and MBI. **SM2** shows strong ICT effect to provide the peaks at 581-601 nm, which is caused by the effective electron deficient MBI unit with 1,2-quinoid form.[20] But **SM1** does not show absorption peak in this reason showing that PT unit is not an effective electron withdrawing unit to provide ICT effect. In contrast to the MBI unit with 1,2-quinoid form, with two electron pulling imine groups directly attached to the conjugated backbone, the PT unit has thiadiazole unit with two imine groups isolated from conjugated biphenyl backbone. In comparison with the absorption spectra of the solutions, absorption spectrum of the thin film of **SM2** shows shift to a longer wavelength region by 18-20 nm.

Electrochemical Properties of the Small Molecules. The cyclic voltammetry (CV) was performed with a solution of 0.1 M of TBAP in methylene chloride at a scan rate of 100 mV/s at room temperature. A platinum electrode, Pt wire and $Ag/AgNO_3$ electrode were used as the working, counter and reference electrode, respectively. The energy level of the $Ag/AgNO_3$ reference electrode (calibrated by the FC/FC^+ redox system)

Table II. Electrochemical Potentials and Energy Levels of SM1 and SM2

Donor	Optical Band Gap[a] (eV)	HOMO[b] (eV)	LUMO[c] (eV)	E_{ox}[d] (V)
SM1	2.68	-5.15	-2.47	0.75
SM2	1.64	-5.85	-4.21	1.45

[a]Optical energy band gap was estimated from the onset wavelength of the optical absorption. [b]Calculated from the oxidation potentials. [c]Calculated from the LUMO=HOMO+E_g^{opt}. [d]Onset oxidation and reduction potential measured by cyclic voltammetry.

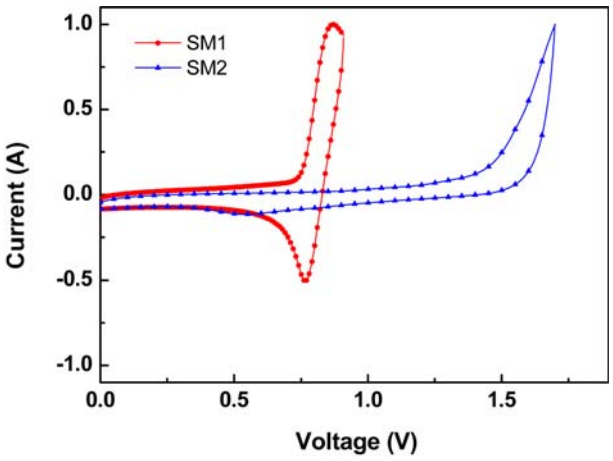

Figure 4. Cyclic voltammetry curves of the small molecules in 0.1 M TBAP in methylene chloride solution at a scan rate of 100 mV/s at room temperature (*vs*. an Ag quasi-reference electrode).

was 4.4 eV below the vacuum level. The electrochemical data of the materials are summarized in Table II. The highest occupied molecular orbital (HOMO) levels was calculated according to the empirical formula (E_{HOMO}=-([E_{onset}]^{ox}+4.4) eV) from CV and the corresponding lowest unoccupied molecular orbital (LUMO) levels were estimated from LUMO=HOMO+E_g^{opt}. The small molecules, **SM1** and **SM2**, exhibited the absorption onset wavelengths of 463 and 756 nm in solid thin films, which corresponds to the bandgaps of 2.68 and 1.64 eV, respectively. The small molecules exhibit irreversible processes in an oxidation scan. As shown in Figure 4, the oxidation onsets of the small molecules, **SM1** and **SM2**, were estimated to be 0.75 and 1.45 V, which correspond to HOMO energy levels of -5.15 and -5.85 eV, respectively. **SM2** showed a deeper HOMO level, which is in the ideal region for ensuring oxidative stability and generating a higher V_{OC}.[21] The estimated LUMO energy level of **SM1** and **SM2** were -2.47 and -4.21 eV, respectively.

The optimized geometry and the HOMO and LUMO energy levels were calculated at the B3 LYP/6-311+G level of theory using the Gaussian 03 package,[22] as shown in Figure 5. The HOMO and LUMO surfaces were plotted using the GaussView version 4.1. To simplify the calculations, the alkyl chains were replaced by methyl groups. For **SM1**, the HOMO is mainly distributed on the BDT unit (the electron rich unit), while the LUMO on the PT unit (the electronic deficient unit), suggesting that **SM1** is a typical D-A type. The calculated HOMO and LUMO energy levels are -5.64 and -2.78 eV, respectively, giving an band gap of 2.86 eV. The feature out of the same calculation of **SM2** shows that there is more electron distribution in the MBI portion, electron deficient unit, to provide better ICT. The calculated HOMO energy level is -5.23 eV, while that of LUMO is -3.33 eV, giving a band gap of 1.9 eV. The comparison of these computed results shows that **SM2** has a lowerlying LUMO, which is consistent with the LUMO energy levels estimated from LUMO=HOMO+E_g^{opt}. In **SM1**, the dihedral angles between the two BDT and PT unit are 23.9° and 14.6°. In case of **SM2**, the dihedral angles are 1.5° and 21.6° between the two BDT and MBI units. The smaller dihedral angles results in better ICT effect in case of **SM2** as compared to the case of **SM1**.[23]

OFET (Organic field-effect transistor) and Photovoltaic Properties of the Small Molecules. The field-effect carrier mobilities of the small molecules were measured by fabricating thin film field-effect transistors (FETs) using the top-contact geometry. The Figure 6 shows the FET transfer characteristics of the small molecules devices of the OTS-modified SiO_2. Hole mobilities of the **SM1** and **SM2** were calculated from the transfer characteristics of the OFETs. The field-effect hole mobilities of **SM1** and **SM2** are 1.06×10^{-6} and 1.42×10^{-6} cm^2/Vs, respectively. Since there is no small molecules which have BDT and BT units, polymers with BDT and BT units could be compared with **SM1** and **SM2**. Even though small molecules provide lower mobility as compared to the corresponding polymers in most of the cases, the field-effect hole mobilities of **SM1** and **SM2** are comparable or even higher than these polymers.[24]

The photovoltaic properties of **SM1** and **SM2** were investigated by fabricating the OPVs with ITO as positive electrode, the blend with small molecules (**SM1** and **SM2**) and PCBM as active layer, and Al as negative electrode. Figure 7 shows the current-voltage (*I-V*) curves of the OPVs with the configuration of ITO/PEDOT:PSS/small molecule:PCBM/Al under AM1.5G irradiation (100 mW/cm^2) and summarized in Table III. Bulk hetero junction (BHJ) devices were fabricated by spin-coating of 1% (w/v) ODCB solutions comprising a blend of small molecule and PCBM in different blend ratios (2:8 and 3:7). The devices with **SM1** and PCBM with ratio of 3:7 showed a V_{OC} of 0.77 V, a J_{SC} of 0.61 mA/cm^2, and a fill factor (*FF*) of 0.30, giving a power conversion efficiency of 0.15%. The devices comprising **SM2** with PCBM (3:7) showed a V_{OC} of 0.62 V, a J_{SC} of 1.69 mA/cm^2, and a fill factor (FF) of 0.27, giving a power conversion efficiency of 0.28%. The **SM1** device had poor performance because of its bigger dihedral angles between the two BDT

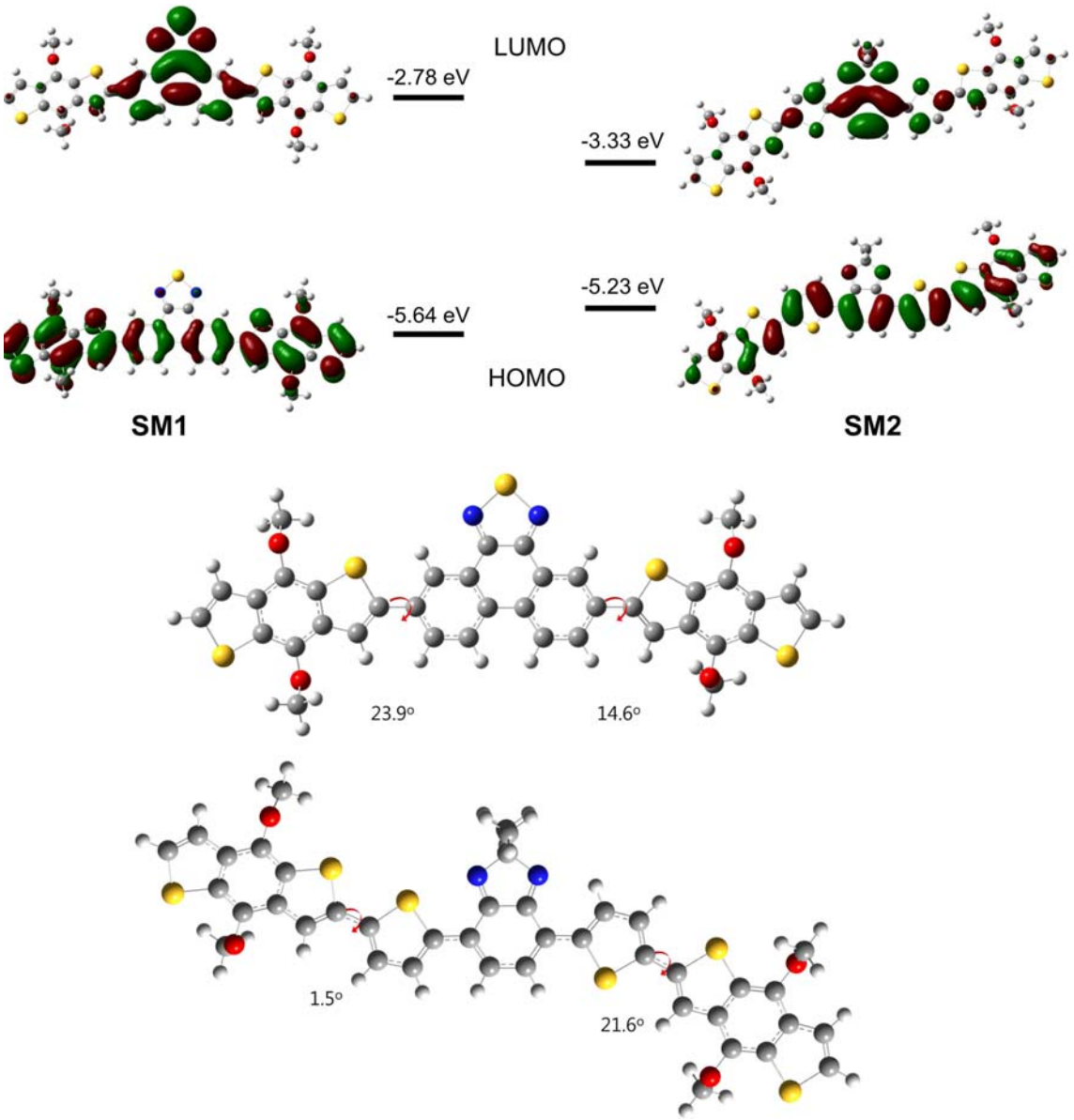

Figure 5. The HOMO and LUMO of BTI, SM1 and SM2 at the B3LYP/6-311+G level of theory.

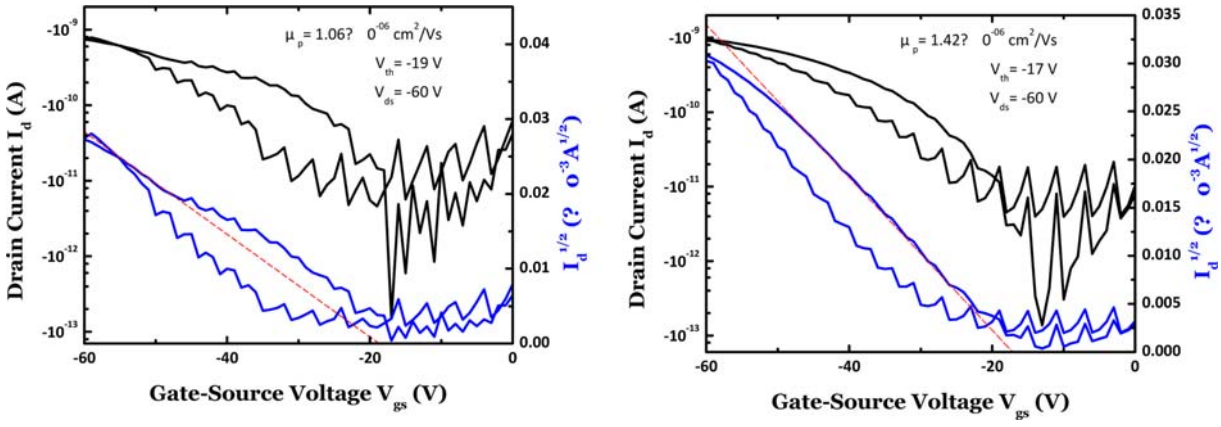

Figure 6. OFET properties of **SM1** and **SM2**.

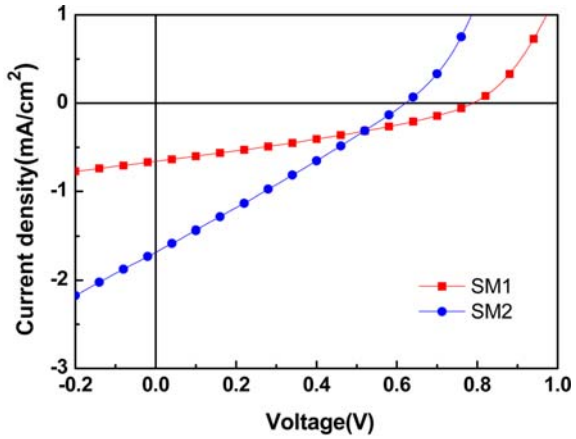

Figure 7. Current density-potential characteristics of the **SM1**:PCBM =3:7 and **SM2**:PCBM=3:7 under the illumination of AM 1.5, 100 mW/cm^2.

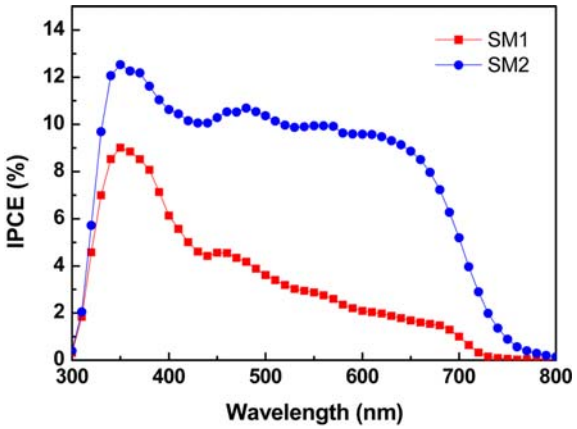

Figure 8. IPCE curves of the **SM1**:PCBM=3:7 and **SM2**:PCBM=3:7 under the illumination of AM 1.5, 100 mW/cm^2.

and PT units and the poor the morphology, as shown in Figure 9(a). The incident-photon-to-current efficiency (IPCE) spectra of the photovoltaic devices from small molecule:PCBM blends are presented in Figure 8. The IPCE spectra of the small molecules show maxima of 12.5% at 349 nm for **SM2** and 9.0% at 351 nm for **SM1**. The enhanced efficiency of **SM2** results from the higher IPCE values between 300 and 750 nm. The higher IPCE values of **SM2** led to a larger current density than that of **SM1**, which is caused by the higher absorption

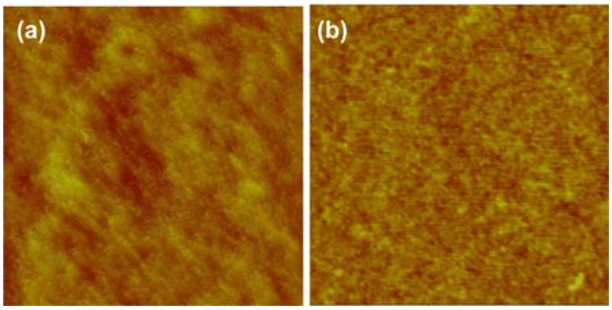

Figure 9. Atomic force microscopy images of **SM1**:PCBM=3:7 (a) and **SM2**:PCBM=3:7 (b).

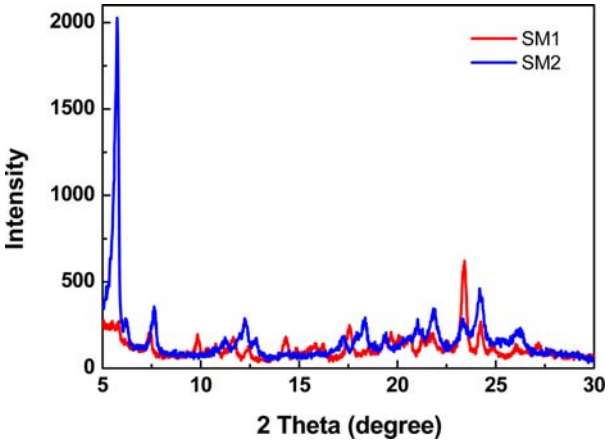

Figure 10. XRD (X-ray diffraction) images of **SM1** and **SM2**.

in the longer wavelength range. Atomic force microscopy (AFM) studies of material blends (**SM1**:PCBM=3:7 w/w and **SM2**:PCBM=3:7 w/w) revealed that the morphology of the small molecule/PCBM blend films exhibited very fine domains and no large phases can be found in Figure 9, where the images were obtained in a surface area of 2.5×2.5 μm^2 by the tapping mode. The AFM image of **SM1** and **SM2** exhibit a root-mean-square (rms) roughness of 0.24 nm and 0.96 nm, as shown in Figure 8. The highly ordered crystalline domain and improved surface roughness can contribute for the better pathways for electrons and holes and increase the J_{SC} values.[25] As shown in Figure 10, the diffraction result reveals that the **SM2** shows peak with high intensity suggesting highly ordered crystalline domain as compared to **SM1**.[26-28]

Table III. Photovoltaic Properties of SM1 and SM2[a]

Donor	Donor:PCBM (ratio)	V_{OC} (V)	J_{SC} (mA/cm^2)	FF	PCE (%)
SM1	2:8	0.79	0.66	0.29	0.11
	3:7	0.77	0.61	0.30	0.15
SM2	2:8	0.65	0.89	0.26	0.15
	3:7	0.62	1.69	0.27	0.28

[a]Concentration 33 mg/mL.

Conclusions

Two small organic molecules, **SM1** and S**M2** with BDT as the electron rich unit and MBI/PT as the electron deficient units, were synthesized by Stille coupling reaction with Pd(0)-catalyst to provide good solubility in common organic solvents. The solution and the solid thin film of **SM1** present absorption bands with maximum peaks at 362 and 367 nm, respectively. As compared to this, the solution and the solid thin film of **SM2** provided absorption bands with maximum peaks at 368, 581 and 381, 601 nm, respectively, including the long wavelength peaks caused by the ICT effect. Solution-processed OPVs with **SM1** and **SM2** as donor and PCBM as acceptor were fabricated, and the experimental conditions with different blending ratios were optimized. The devices comprising **SM2** with PCBM (3:7) showed a V_{OC} of 0.62 V, a J_{SC} of 1.69 mA/cm^2, and a fill factor (FF) of 0.27, giving a power conversion efficiency of 0.28%.

Acknowledgment. This work was supported by a 2-Year Research Grant of Pusan National University.

References

(1) L. Dou, C. C. Chen, K. Yoshimura, K. Ohya, W. H. Chang, J. Gao, Y. Liu, E. Richard, and Y. Yang, *Macromolecules*, **46**, 3384 (2013).
(2) M. Seri, M. Bolognesi, Z. Chen, S. Lu, W. Koopman, A. Facchetti, and M. Muccini, *Macromolecules*, **46**, 6419 (2013).
(3) Q. Shi, P. Cheng, Y. Li, and X. Zhan, *Adv. Energy Mater.*, **2**, 63 (2012).
(4) Z. Lu, C. Li, T. Fang, G. Lia, and Z. Bo, *J. Mater. Chem. A*, **1**, 7657 (2013).
(5) A. Tang, L. Li, Z. Lu, J. Huang, H. Jia, C. Zhan, Z. Tan, Y. Lib, and J. Yao, *J. Mater. Chem. A*, **1**, 5747 (2013).
(6) S. Roquet, A. Cravino, P. Leriche, O. Alévêque, P. Frère, and J. Roncali, *J. Am. Chem. Soc.*, **128**, 3459 (2006).
(7) H. Shang, H. Fan, Y. Liu, W. Hu, Y. Li, and X. Zhan, *J. Mater. Chem.*, **21**, 9667 (2011).
(8) A. B. Tamayo, X. D. Dang, B. Walker, J. Seo, T. Kent, and T. Q. Nguyen, *Appl. Phys. Lett.*, **94**, 103301 (2009).
(9) B. Walker, A. B. Tamayo, X. D. Dang, P. Zalar, J. H. Seo, A. Garcia, M. Tantiwiwat, and T. Q. Nguyen, *Adv. Funct. Mater.*, **19**, 3063 (2009).
(10) J. Zhang, Y. Yang, C. He, Y. He, G. Zhao, and Y. Li, *Macromolecules*, **42**, 7619 (2009).
(11) H. Shang, H. Fan, Y. Liu, W. Hu, Y. Li, and X. Zhan, *Adv. Mater.*, **23**, 1554 (2011).
(12) W. Ying, X. Zhang, X. Li, W. Wu, F. Guo, J. Li, H. Agren, and J. Hua, *Tetrahedron*, **70**, 3901 (2014).
(13) J. Min, Z. G. Zhang, S. Zhang, M. Zhang, J. Zhang, and Y. Li, *Macromolecules*, **44**, 7632 (2011).
(14) S. Song, S.H. Park, Y. Jin, J. Park, J.Y. Shim, I. Kim, H. Lee, K. Lee, and H. Suh, *J. Polym. Sci. Pol. Chem.*, **48**, 4567 (2010).
(15) S. Song, S.H. Park, Y. Jin, I. Kim, K. Lee, and H. Suh, *Polymer*, **51**, 5385 (2010).
(16) W. Zhang, J. Smith, S.E. Watkins, R. Gysel, M. McGehee, A. Salleo, J. Kirkpatrick, S. Ashraf, T. Anthopoulos, M. Heeney, and I. McCulloch, *J. Am. Chem. Soc.*, **132**, 11437 (2010).
(17) H. N. Tsao, D. Cho, J.W. Andreasen, A. Rouhanipour, D.W. Breiby, W. Pisula, and K. Müllen, *Adv. Mater.*, **21**, 209 (2009).
(18) J. E. Carlé, J. W. Andreasen, M. Jørgensen, and F. C. Krebs, *Sol. Energy Mater. Sol. Cells*, **94**, 774 (2010).
(19) S. Song, S. Park, S. Kwon, B. H. Lee, J. Y. Shim, J. Lee, S. H. Park, Y. Jin, I. Kim, K. Lee, and H. Suh, *Sol. Energ. Mat. Sol. C.*, **105**, 229 (2012).
(20) T. H. Lee, K. Y. Wu, T. Y. Lin, J. S. Wu, C. L. Wang, and C. S. Hsu, *Macromolecules*, **46**, 7687 (2013).
(21) J. H. Kim, C. E. Song, B. S. Kim, I. N. Kang, W. S. Shin, and D. H. Hwang, *Chem. Mater.*, **26**, 1234 (2014).
(22) M. J. Frisch, *et al*., Gaussian 03, Revision E.01, Gaussian Inc., Wallingford, 2004.
(23) C. Y. Mei, L. Liang, F. G. Zhao, J. T. Wang, L. F. Yu, Y. X. Li, and W. S. Li, *Macromolecules*, **46**, 7920 (2013).
(24) C. C. Robert, M. M. N. Christopher, D. P. Eric, W. W. Jeremy, W. O. Jack, A. M. L. Claire, M. S. Gregory, E. N. Ronald, D. J. Oana, and L. C. L. David, *J. Nanotechnol.*, **572329**, 10 (2011)
(25) M. L. Keshtov, D. V. Marochkin, V. S. Kochurov, A. R. Khokhlov, E. N. Koukaras, and G. D. Sharma, *J. Mater. Chem. A*, **2**, 155 (2014).
(26) X. Wang, P. Jiang, Y. Chen, H. Luo, Z. Zhang, H. Wang, X. Li, G. Yu, and Y. Li, *Macromolecules*, **46**, 4805 (2013).
(27) M. L. Keshtov, D. V. Marochkin, V. S. Kochurov, A. R. Khokhlov, E. N. Koukaras, and G. D. Sharma, *Polym. Chem.*, **4**, 4033 (2013).
(28) Y. Li, L. Chen, Y. Chen, C. Li, P. Zhang, L. Gao, X. Yang, Y. Tu, and X. Zhu, *Sol. Energy Mater. Sol. Cells*, **108**, 136 (2013).